



The differences of viscoelastic properties between the secondary wall S_2 layer and compound middle lamella of thermally treated wood

Dong Wang¹ · Elin Xiang² · Feng Fu² · Lanying Lin²

Received: 30 August 2021 / Accepted: 16 August 2022 / Published online: 2 September 2022
© The Author(s), under exclusive licence to Springer-Verlag GmbH Germany, part of Springer Nature 2022

Abstract

Thermal modification is a well-established method to improve the dimensional stability and the durability of wood for outdoor use. In this study, samples were thermally treated at 160–220 °C for 1 h. The differences of viscoelastic properties between the cell wall S_2 layer and compound middle lamella (CML) of thermally treated wood were investigated by creep compliance testing and dynamic modulus mapping of nanoindentation. The elastic parameters of the S_2 and CML, such as reduced modulus and storage modulus, decrease and then increase as the treatment temperature increases. By contrast, the loss moduli and loss factors of the two layers decrease steadily as the treatment temperature increases. In addition, the creep compliance results indicate that the S_2 layers of the untreated and treated samples exhibit greater elasticity than does the CML, but the rheological characteristics of the CML are more obvious. Finally, the loss modulus and loss factor of the S_2 layer are also larger than those of the CML. The changes of viscoelastic properties of cell walls of thermally treated wood are mainly related to hemicellulose degradation, the cross-linkage structure between cellulose and matrix breakage, and cellulose microfibrils arrangement.

✉ Lanying Lin
linly@caf.ac.cn

Dong Wang
wdwangdong@nwpu.edu.cn

Elin Xiang
xiangelin@163.com

Feng Fu
feng@caf.ac.cn

¹ Northwestern Polytechnical University of Culture and Heritage, Shaanxi 710072, China

² Research Institute of Wood Industry, Chinese Academy of Forestry, Beijing 100091, China

Introduction

As a lightweight renewable natural composite material, wood is widely used for many purposes due to its high strength-to-weight ratio, excellent workability, and aesthetic appeal. Its utilization is restricted, however, by its lack of dimensional stability, low resistance to decay, and poor durability (Guo et al. 2015; Mastouri et al. 2021). Among various techniques for overcoming these problems, thermal treatment provides an efficient and ecofriendly strategy to improve the dimensional stability and durability of wood (Esteves and Pereira 2009; Laine et al. 2016). The commercial production of thermally treated wood usually takes place in the temperature range 160–240 °C (Hill 2006). The enhanced characteristics of thermally treated wood contribute to its popularity for use in many outdoor applications.

Changes in the mechanical properties (Bekhta and Niemz 2003; Windeisen et al. 2009; Rautkari et al. 2014; Kačíková et al. 2013; Candelier et al. 2016), physical properties (Ding and Li 2011), and chemical properties (Chen et al. 2018; Esteves et al. 2008; Rautkari et al. 2014) of thermally treated wood have been extensively investigated. When being thermally treated, wood undergoes a series of chemical transformations, including the degradation of hemicellulose, cross-linking of lignin, and crystallization of cellulose (Chen et al. 2018; Esteves et al. 2008; Rautkari et al. 2014). In addition, the cellulose of thermally treated wood is degraded slightly in the secondary wall and compound middle lamella (CML), especially in the cell corner regions, and β -aryl-ether links associated with guaiacyl units of lignin are depolymerized followed by re-condensation reactions (Yin et al. 2011, 2017). The effects of changes in chemical structure on the mechanical properties of wood after thermal treatment have also been widely studied (Ding and Li 2011).

Much of the current research is focused on finding out more about the mechanical properties of thermally treated wood from the macro scale to the nanometer scale (Guo et al. 2015; Li et al. 2017; Tjeerdsma and Militz 2005). It has been found that compression strength and modulus of rupture decrease as exposure duration and temperature increase (Yildiz et al. 2006). Treatment of wood at high temperatures results in a reduction in toughness and an increase in brittleness (Gong et al. 2010; Esteves and Pereira 2009).

Nanoindentation has been widely used to characterize the stiffness, hardness, creep, and viscoelastic properties of thermally treated wood cell walls at the sub-micrometer scale (Wang et al. 2014; Wu et al. 2019; Stanzl-Tschegg et al. 2009). Xiang et al. (2021) and Xing et al. (2021) discussed the effect of thermal treatment on creep of the S_2 layer of the cell wall by nanoindentation creep testing, and demonstrated that both the creep ratio and maximum creep compliance of thermally treated wood decreased. Viscoelastic deformation energies of the cell wall S_2 layer also show a significant decrease with increasing temperature of thermal treatment, which characterizes viscoelastic creep during the holding period of the indentation test (Stanzl-Tschegg et al. 2009). Most of the previous studies focused on the changes of the viscoelastic properties of the cell wall S_2 layer of

thermally treated wood, with differences between layers of cell wall, especially the S_2 and CML, being largely ignored. Although the CML is weaker than the S_2 layer, it provides an important set of interfaces in wood, strongly affecting the wood's plastic and creep deformations (Barthelat et al. 2016). Furthermore, the mechanisms of viscoelastic changes after thermal treatment between the S_2 and CML are also different because of their differences in chemical composition.

The objective of this study is to evaluate the differences in the viscoelastic properties of the S_2 and CML of thermally treated wood. Creep tests and dynamic modulus mapping of nanoindentation conducted in this study should help to further elucidate the differences of viscoelastic parameters between the S_2 and CML of thermally treated wood. Furthermore, clarifying the influence of thermal treatment on the viscoelastic properties of these layers may also be interesting for further understanding viscoelasticity of thermally treated wood at the cellular scale.

Materials and methods

Materials

A quarter-sawn board of spruce wood (*Picea asperata* Mast.) was acquired from Shanghai Chengjia Wood Industry Co., LTD, China. A board with dimensions of 350 mm × 200 mm × 20 mm (longitudinal × tangential × radial) was prepared for the experiments. The board was arbitrarily divided into three specimens. The average moisture content of the sample was 13.9% and its basic density was 0.41 g/cm³.

Methods

Thermal treatment

Specimens were treated thermally in a vacuum vessel equipped with two metal heating plates for 1-h successive periods at 160, 180, 200, and 220 °C, as described in a previous study (Wang et al. 2022). First, specimens were clamped between two metal heating plates. Then, residual gas was removed from the vessel by pulling a vacuum of -0.9 MPa for 1 h. The two metal heating plates were heated to the predetermined temperature at a heating rate of 30 °C/min. Then, the specimen was held for about 15 min to allow its center temperature to reach the heating-plate temperature. Treatment time was set to be 1 h. Finally, the vacuum was released, and the specimens were taken out.

Chemical constituents

The untreated and treated wood specimens were ground into powders with particle sizes between 40 and 60 mesh using a Wiley mill. The holocellulose content was measured following the GB/T 747–2003 standard method, and the cellulose content

was determined from the α -cellulose content according to the GB/T 744–1979 standard method. The hemicelluloses content was calculated using the difference between holocellulose and α -cellulose. Three replicates were performed for each group.

XRD measurements

The untreated and treated wood samples were milled to fine powders and passed through a 60-mesh screen. The XRD patterns of the samples were measured using an X-ray diffractometer (D8 Advance, BRUKER, Germany), with Ni-filtered CuK α radiation ($\lambda=0.154$ nm) at 40 kV and 40 mA. The reflection intensity was recorded through a scanning-angle (2θ) range of 5° to 45° at a scanning speed of $1^\circ/\text{min}$. The background was subtracted, and peaks were resolved using PeakFitR (Sea-Solve Software Inc., Richmond, CA, USA). The crystallinity index (CI), or relative crystallinity, was calculated by the Turley method, as follows:

$$CI = \frac{I_{002} - I_{am}}{I_{002}} \times 100\% \quad (1)$$

where I_{002} is the maximum intensity at the diffraction angle of the 002 plane and I_{am} is the minimum intensity corresponding to the amorphous cellulose fraction. The crystal dimension D_{hkl} was evaluated using the Scherrer equation,

$$D_{hkl} = \frac{K\lambda}{\beta_{1/2}\cos\theta} \quad (2)$$

where K is the Scherrer constant ($K=0.9$), λ is the X-ray wavelength, $\beta_{1/2}$ is the peak full-width-at-half maximum intensity ($\text{FWHM}=2^\circ$), and θ is the diffraction angle.

Viscoelastic properties

Creep tests using nanoindentation technology combined with the Burger model provide a method for studying the elasticity, viscoelasticity, and viscosity of wood cell walls (Meng et al. 2015; Wang et al. 2019). For nanoindentation creep tests, the holding segment of the load-depth curve was analyzed, and the creep compliance $J(t)$ was defined as

$$J(t) = \frac{A(t)}{2(1-\nu^2)P_0\tan\delta} \quad (3)$$

where ν is Poisson's ratio of the cell wall ($\nu=0.21$), δ is the half-open angle of the indenter, and P_0 is the holding load. The contact area $A(t)$ is strongly related to the

indentation depth and is calculated by the area function of the tip, as described in a previous study (Wang et al. 2019).

The Burger model has previously been applied to rationalize experimental results and to investigate the wood cell wall (Meng et al. 2015; Wang et al. 2019). With reference to the Burger model, a combination of a Maxwell and a Kelvin element was used, as indicated in the schematic diagram shown in Fig. 1. An equation of creep compliance can be written as:

$$J(t) = J_0 + J_1 \cdot t + J_2[1 - \exp(-t/\tau_0)] \quad (4)$$

where $J_0 = \frac{1}{K_1}$, $J_1 = \frac{1}{\eta_1}$, $J_2 = \frac{1}{K_2}$, and $\tau_0 = \frac{\eta_2}{K_2}$. τ_0 is the retardation time, which describes the retarded elastic deformation of the Kelvin model in the Burger model and reflects the viscoelastic properties of wood cell walls.

The creep compliance test was conducted using a nanoindentation instrument with a Berkovich diamond pyramid tip (TI 950 Triboindenter, Hysitron, Inc., tip angle = 142.3°). Prior to the indentation test, samples were stored in the indentation chamber and equilibrated for 24 h at 21 °C and 65 ± 4% relative humidity. A load function of 5 s–50 s–5 s (loading, holding, and unloading) with a maximum load of 100 μN was used for the measurements. The creep compliances of the S₂ and CML layers were measured and calculated using Eq. (3) (see Fig. 1). Then, using Eq. (4), nonlinear curve fitting was used to analyze the creep compliance data with Origin 8.5 software; the correlation coefficient R^2 was found to be more than 0.99. Finally, the elastic, viscoelastic, and viscosity parameters of the treated wood cell walls were obtained. In addition, the reduced modulus and hardness were calculated from the unloading segment (Fig. 1). To ensure the reliability of the experimental results, at least 25 indentation measurements were conducted for each group of samples.

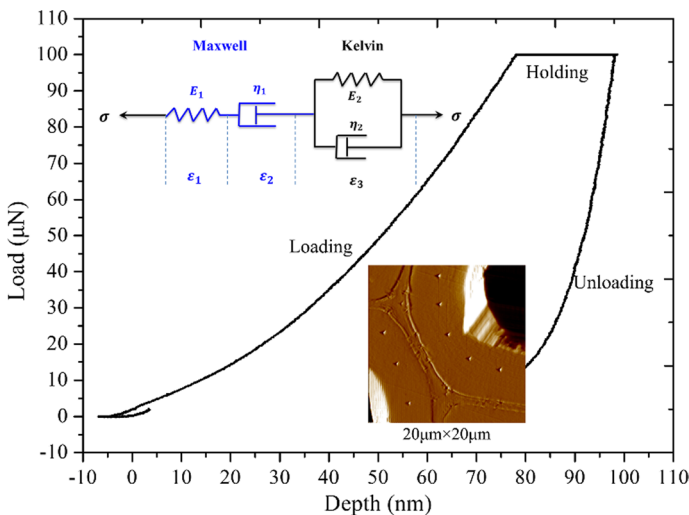


Fig. 1 Load-depth curve obtained from nanoindentation tests and Burger model

Dynamic viscoelastic properties

The dynamic viscoelastic properties of the thermally treated wood cell walls were examined using dynamic modulus mapping from nanoindentation (TI 950 Triboindenter, Hysitron, Inc.). To reduce the effect of roughness on modulus measurements, the surface roughness was reduced to 10 nm or less by using new diamonds during the cutting process. The cross-sectional area ($10\ \mu\text{m} \times 10\ \mu\text{m}$) of the tangential double walls of the treated latewood was chosen as the region of interest. While scanning the sample surface, an appropriate dynamic force, sensitivity, and time constant were chosen in the lock-in control window to obtain an amplitude plot of about 0.90–1.20 nm. The frequency of the oscillation applied to the probe during imaging was 200 Hz, and the dynamic force was 0.4 μN . The sensitivity was 50 mV and the time constant 3 ms. The tip radius was calibrated by the reduced modulus of nanoindentation during the modulus analysis. The complex modulus (CM), storage modulus (SM), and loss modulus (LM) mapping images of the cell walls of the treated wood were obtained.

Results and discussion

Chemical constituents

The results for the chemical constituents of the thermally treated samples are shown in Table 1. The hemicellulose began to degrade at 160 °C, consistent with the results of Li et al. (2017). One-factor ANOVA was used to investigate the statistical significance of the relative chemical compositions as a function of temperature (Table 1). The results indicate that the hemicellulose is significantly degraded with higher-temperature treatment, but for the cellulose almost no degradation occurred. The main reason is that cellulose has better thermal stability than hemicellulose (Shen et al. 2010). Finally, the degradation of hemicellulose after thermal treatment led to significant increase in the relative content of lignin. Similar results have been reported by others (Tümen et al. 2010).

Table 1 Chemical constituents, crystallinity (CI), and crystallization width (D_{002}) of thermally treated wood

| Samples | Lignin (%) | Cellulose (%) | Hemicellulose (%) | CI (%) | D_{002} (nm) |
|-----------|---------------------------|---------------------------|---------------------------|----------------------------|--------------------------|
| Untreated | 21.65 ^D (0.31) | 43.65 ^A (0.29) | 24.74 ^A (0.45) | 48.32 ^D (0.32) | 2.79 ^D (0.02) |
| 160 °C | 22.70 ^C (0.12) | 43.89 ^A (0.59) | 21.66 ^B (0.34) | 49.48 ^C (0.06) | 2.83 ^C (0.01) |
| 180 °C | 22.77 ^C (0.88) | 43.68 ^A (0.11) | 21.18 ^C (0.23) | 52.54 ^B (0.19) | 2.90 ^B (0.02) |
| 200 °C | 23.55 ^B (0.07) | 43.47 ^A (0.19) | 20.69 ^D (0.30) | 53.96 ^A (1.08) | 2.95 ^A (0.03) |
| 220 °C | 24.97 ^A (0.13) | 42.98 ^A (0.77) | 18.41 ^E (0.64) | 53.27 ^{AB} (0.70) | 2.97 ^A (0.02) |

Superscripts A, B, C, D denote analysis of variance, where the same letter indicates no statistically significant difference between different treatment temperatures at a significance level of 5%

Cellulose crystalline structure

XRD patterns of the untreated and treated samples are shown in Fig. 2. After thermal treatment, there was a significant increase in the intensity of the (200) reflection, especially in the 180–200 °C treated samples. However, the intensity for the 220 °C treated sample is less than that of the 200 °C treated wood. Interestingly, the (004) reflection shows no difference between the untreated and treated woods, suggesting that the cellulose molecular chains remained largely unaffected by the 160–220 °C temperatures.

As shown in Table 1, the crystallinity and crystal width of thermally treated samples are greater than those of untreated samples. In addition, the *CI* values of samples at 160–200 °C increased from 49.48% to 53.96%, which is similar to variations in the *CI* after heating in air or nitrogen (Kuboijima et al. 1998). The ANOVA analysis results show that thermal treatment at 160–200 °C has a clear influence on the *CI* at a significance level of 5%. The main reasons for this are hemicellulose degradation and the rearrangement of amorphous cellulose molecules (Hori and Wada 2005; Xing et al. 2016; Yin et al. 2017). Moreover, there was a slight decrease in the crystallinity at 220 °C, but it was not a meaningful difference from the value at 200 °C at a significance level of 5%. Furthermore, the crystallite thickness (D_{200}) of the untreated wood was 2.77 nm, and the values of the thermally treated samples at 160–220 °C increased from 2.83 nm to 2.97 nm. The ANOVA analysis shows that the treatment temperature has an influence on the cellulose crystallite dimensions at a significance level of 5%, which is in agreement with the results of Wang et al. (2018).

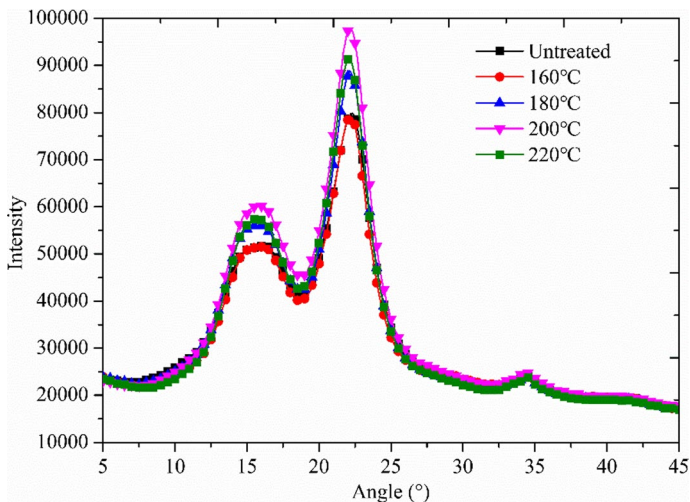


Fig. 2 X-ray diffraction patterns of thermally treated and untreated samples

Reduced modulus of cell wall layers

The basic evaluation of nanoindentation creep tests reveals that the reduced modulus of cell walls is dependent on the thermal treatment temperature (Fig. 3). For both untreated and treated samples, the reduced modulus of the S_2 layer was more than that of the CML. The main reasons for this are that the highest level of lignin concentration occurs in the CML, while the highest level of cellulose is found in the S_2 layer, and the cellulose microfibril arrangement in this layer is parallel to the cell axis (Wang et al. 2019). Furthermore, the thermal treatment at 160–180 °C led to a decrease in the cell wall modulus, which is in accordance with corresponding softwood data described by Xing et al. (2016). For the 160 °C treated sample, the reduced moduli of the S_2 and CML layers slightly decreased, the amounts of decrease being 4.4% and 7.1%, respectively. However, this effect is not very significant in view of the large scattering of data relative to the untreated sample (Fig. 3). For the 180 °C treated sample, the elastic parameter E_r of the S_2 and CML layers significantly decreased, by 15.6% and 11.6%, respectively. The hemicellulose degradation was a cause of the slight decrease in the indentation modulus. The main reason was that the hemicellulose crosslinked on the surface of the microfibrils and improved the stiffness of the cell wall (Berglund et al. 2020; Wang et al. 2022). Another likely reason is that the morphological changes in cell walls caused by thermal treatment, such as the cleavage of acetyl groups of the hemicellulose, the formation of carbonic acids (Tuong and Li 2010), and the recondensation of the lignin (Nguila Inari et al. 2007) dramatically affect the nanomechanical properties of the cell walls.

However, as the treatment temperature is increased from 180 °C to 220 °C, the reduced modulus of the cell wall increases again (Fig. 3). For example, the modulus

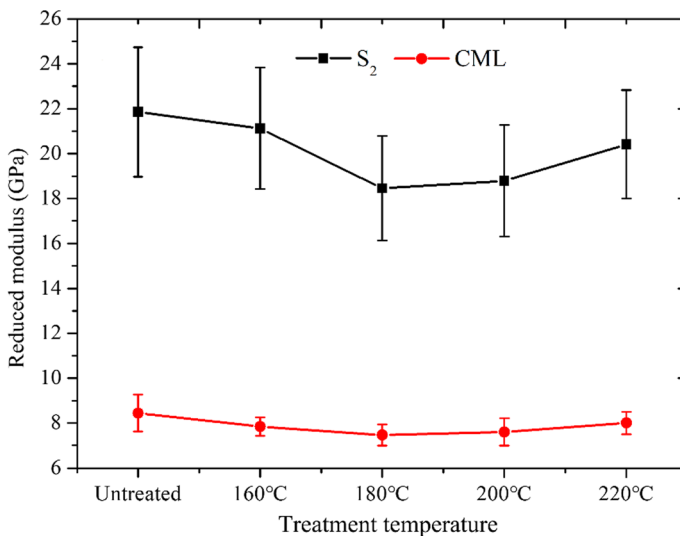


Fig. 3 Dependence of the reduced modulus of the S_2 and CML layers on the treatment temperature

of the S_2 layer increased from 18.45 to 20.41 GPa, consistent with previous results for thermally treated wood at 180–210 °C under N_2 conditions (Xing et al. 2020); and the modulus of the CML increased from 7.47 to 8.01 GPa. The modulus is affected by several factors, such as the cellulose microfibril angle, crystallinity, and the cellulose, lignin, and hemicellulose components of the cell walls. Although the hemicellulose at a treatment temperature of 200 °C was further degraded, the crystallinity of the cell wall increased. Hence, the crystallinity contributes to the modulus of the cell wall. Furthermore, in an earlier study (Wang et al. 2022), the microfibril angle significantly decreased at a treatment temperature of 220 °C, which increased the modulus of the S_2 layer. This indicates that the modulus of the S_2 layer after 220 °C treatment was increased by 10.6%, and was more than that of the CML (7.2%).

Viscoelastic properties of cell walls

The investigation of creep behavior was limited to 50 s of constant loading force, and $J(t)$ creep compliances were determined by means of the indentation holding section data. The experimental creep compliances of the S_2 and CML layers after thermal treatment are illustrated in Fig. 4. For both the treated and untreated samples, the creep compliances of the S_2 (Panel A) and CML (Panel B) increased as the holding times increased. For comparing the data (Fig. 5), the average creep compliance is defined as the area under the creep compliance curve divided by the holding time. The average creep compliance of both layers increases as the treatment temperature increases from 160 to 180 °C, and then decreases as the treatment temperature increases further. The microfibril angle, linkage of lignin, and activation energy are the main factors for the creep behavior of wood cell walls (Gril et al. 2004). With increasing temperature, the hemicellulose first degrades for higher activation energy, which makes the shear slip between cellulose and matrix easier (Jin et al. 2015). The loss of hemicellulose and cross-linkage of lignin aggravates creep of thermally treated samples. However, an earlier study shows that thermal treatment from 200 °C to 220 °C can also lead to reorientation of cellulose microfibrils along the fiber axis (Wang et al. 2022). This reorientation behavior causes the viscous flow and creep behavior of cell walls to decrease.

The slope of the creep compliance curve is the time rate of change of creep, as illustrated in the Supplemental Material (Fig. 1S). The creep rate of the S_2 layer during the first 5 s of holding time is more than that of the CML; after 5 s, the creep rates for both tests tend toward constancy (Fig. 1S). Furthermore, the average creep compliances of the CMLs for all samples, treated and untreated, are more than those of the S_2 layers (Fig. 5). The main reason is that the highest level of lignin concentration occurs in the CML. The viscoelastic behavior is mediated by the lignin, which may entangle and disentangle in the shearing process (Åkerholm and Salmén 2003). For the S_2 layer, the cellulose microfibrils are arranged parallel to the cell axis, leading to a decrease in creep in the S_2 layer (Xing et al. 2016).

The rheological representation of the proposed Burger model is drawn in Fig. 1, with a Maxwell element and a Kelvin element. The Maxwell element is represented

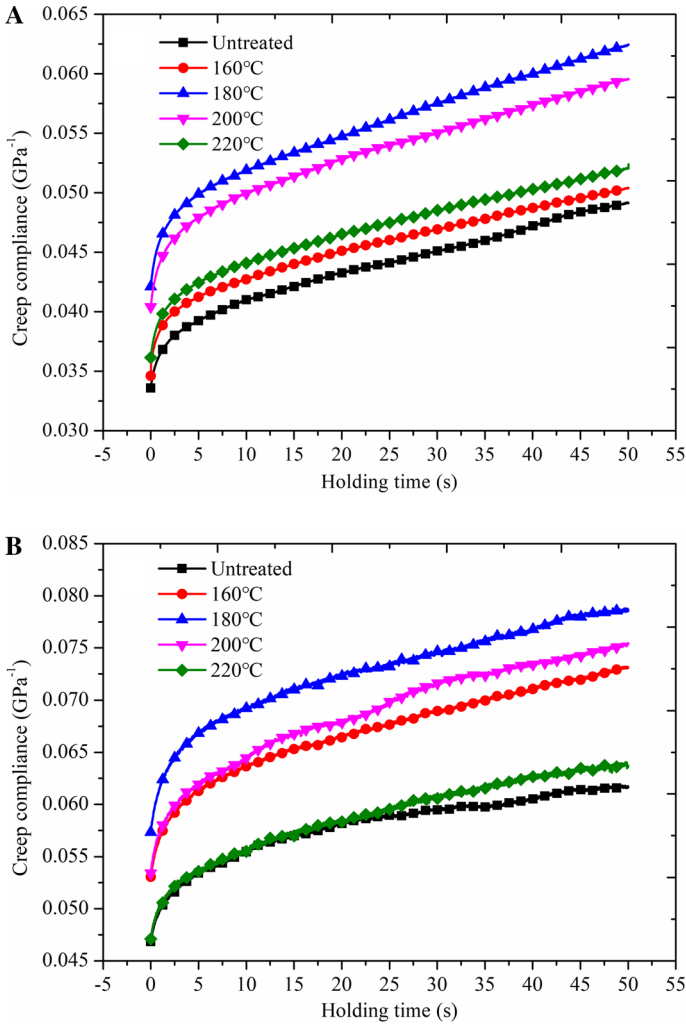


Fig. 4 Creep compliance of thermally treated wood cell walls (**a**: S₂; **b**: CML)

by a spring of rigidity E_1 in series with a parabolic dashpot, characterized by η_1 . The Kelvin element is represented by a spring of rigidity E_2 in parallel with a dashpot (η_2). The two elements are arranged in parallel with respect to the fiber direction. The experimental creep compliance data, together with the Burger model, predicts important viscoelasticity parameters. The correlation coefficient (R^2) was over 0.99 for all samples, indicating that the Burger model is appropriate for predicting the viscoelastic behavior of wood cell walls, as shown in Fig. 2S in Supplementary Material. In the Burger model, the fitting parameters can be physically interpreted as instantaneous elastic deformation followed by viscoelastic deformation and viscous deformation. The parameters in the Burger model are listed in Table 2.

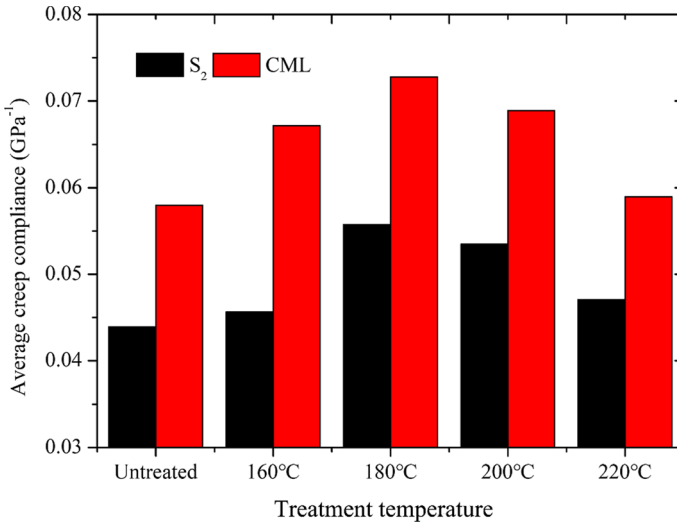


Fig. 5 Average creep compliance of thermally treated wood cell wall S₂ and CML layers

The stiffness parameter (K_1) of the S₂ layers for the untreated and treated samples are greater than those of the CML, and the variation of this parameter with thermal treatment temperature is similar to that of the reduced modulus measured by the nanoindentation test. Moreover, when the stress is constant, the higher the viscosity coefficient (η) the lower the rheology deformation rate $d\epsilon/dt$ (Meng et al. 2015). Hence, the viscosity coefficient (η_1) in the Maxwell element of the S₂ or CML decreases as the thermal treatment temperature increases from 160 °C to 180 °C, indicating an increase in the rate of rheology deformation of thermally treated wood cell walls. The main reasons are that the hemicellulose degradation and the broken cross-linkage between cellulose and matrix lead readily to shear slip between microfibrils. Finally, the reorientation of the microfibrils' long fiber axis by thermal treatment, particularly at 220 °C (Wang et al. 2022), causes η_1 to increase, but the rheology deformation rate to decrease. Finally, according to the data in Table 2, the changes of the parameters of the S₂ and CML layers in the Kelvin element at treatment temperatures are complex.

Dynamic viscoelastic properties

To further study the differences of viscoelastic properties of the S₂ and CML, modulus mapping of nanoindentation was used to test CM, SM, and LM of cell walls in a manner similar to the approach in earlier studies (Qin et al. 2018; Wang et al. 2019). The complex modulus is given as:

$$E = E' + iE'' \quad (5)$$

Table 2 Viscoelasticity parameters of the Burgers model (maximum load 100 μ N, loading time 50 s)

| Parameter (GPa) | Untreated | | 160 °C | | 180 °C | | 200 °C | | 220 °C | |
|--------------------|-----------|---------|---------|---------|---------|---------|---------|---------|---------|---------|
| | S_2 | CML | S_2 | CML | S_2 | CML | S_2 | CML | S_2 | CML |
| K_1 | 28.85 | 20.58 | 27.21 | 18.32 | 22.99 | 16.96 | 23.80 | 17.79 | 26.55 | 20.37 |
| η_1 | 4885.65 | 8445.80 | 4545.46 | 4403.46 | 3779.39 | 4334.33 | 4251.43 | 4406.43 | 5181.06 | 5329.95 |
| K_2 | 229.89 | 136.619 | 222.00 | 135.50 | 168.35 | 116.28 | 168.07 | 123.61 | 204.50 | 171.82 |
| η_2 | 595.39 | 837.65 | 569.80 | 466.20 | 403.59 | 376.37 | 500.77 | 838.60 | 651.02 | 952.08 |

where, E' and E'' are the SM and LM, respectively, and are related to the phase and amplitude.

The moduli CM, SM, and LM of the untreated and treated samples are displayed as a map in Fig. 6. In this map, quantitative values are indicated by different colors. It is evident that the S_2 layer exhibits greater modulus than the CML. Furthermore, there is an obvious transition zone between the S_2 and CML layers, which is related to the secondary wall S_1 layer. It is also interesting that the storage modulus across the thickness of the secondary walls clearly illustrated the gradient distribution near the S_1 and S_2 layers, showing a tendency of decrease from S_2 to S_1 (Fig. 6).

To further evaluate the effect of thermal treatment on storage and loss moduli of wood cell walls, the average E' , E'' and loss factor ($\tan \delta = E''/E'$) of the S_2 and CML layers were calculated from mapping images (Fig. 7). As shown in Fig. 7a, the CM of both the S_2 and CML layers decrease and then increase as the treatment temperature increases, with minima at 180 °C. The variation tendency of the CM is similar to the reduced modulus and creep compliance of the nanoindentation tests, which also relates to the hemicellulose degradation, cross-linkage breakage, and microfibrils reorientation.

The loss modulus E'' of wood is part of the viscous response and generally represents the dissipated energy. The loss moduli and loss factors of the S_2 and CML layers decrease as the thermal treatment temperature increases (Fig. 7b, c). The reason for this is that the connections between hemicellulose, lignin, and cellulose are destroyed at the elevated temperature, and the number of junction points between hemicellulose and cellulose is reduced, which means that the wood cell walls have higher mobility of molecular chains (Wang et al. 2021). This also leads to a decrease in the dissipation energy of interlamellar slip of macromolecules. Moreover, the viscosity of lignin is more prominent than that of polysaccharides (Åkerholm and Salmén 2013). Previous studies have revealed that condensation between lignin fragments can occur during

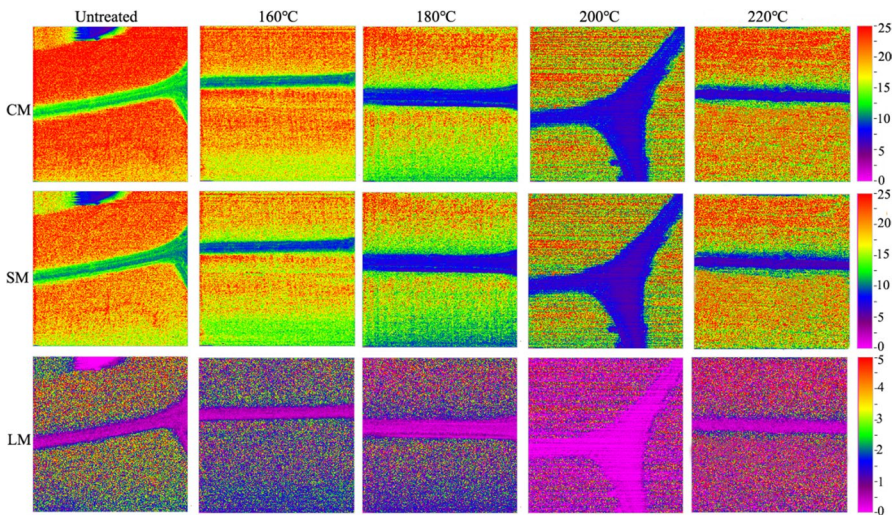


Fig. 6 CM, SM, and LM images for modulus mapping

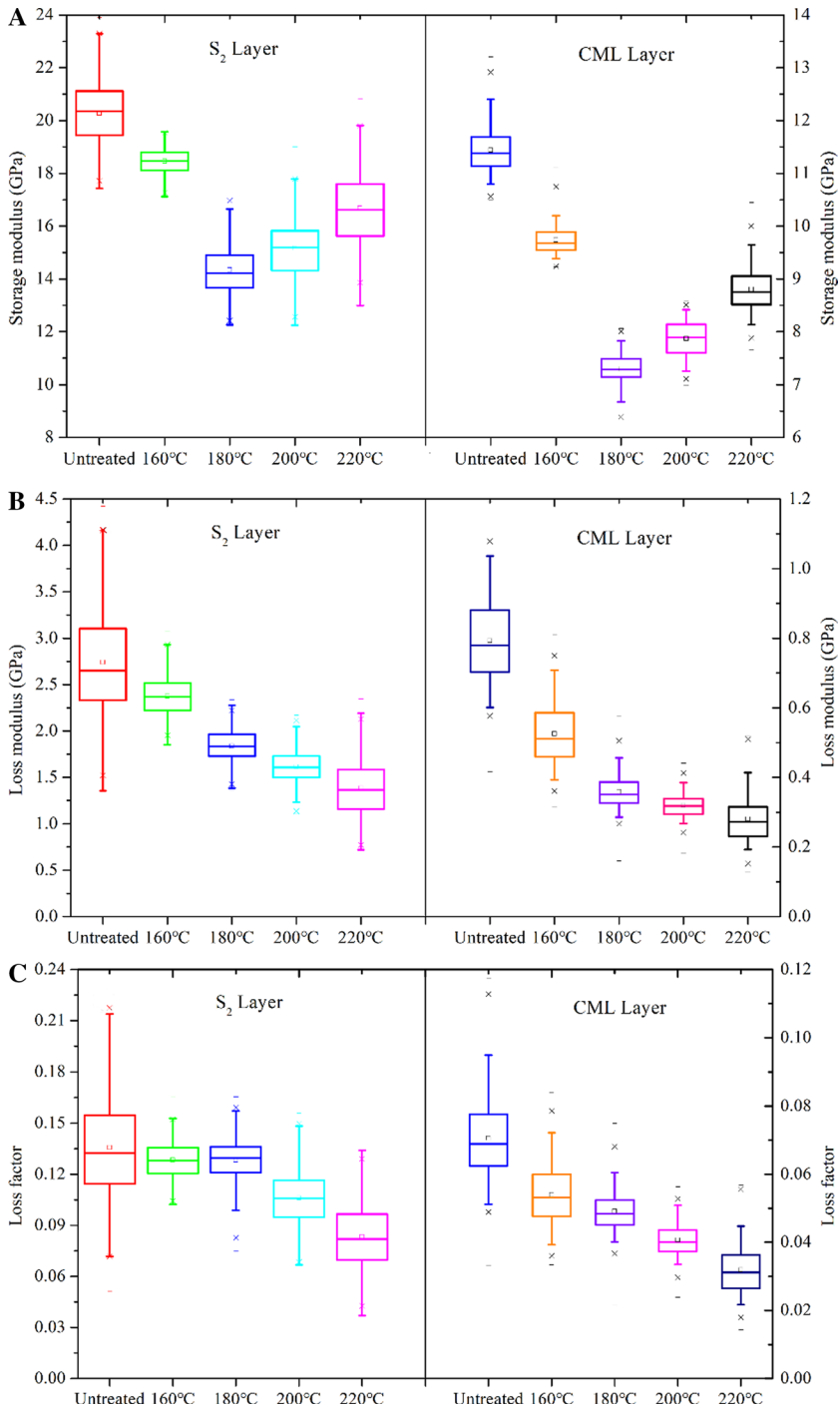


Fig. 7 Dependence of **a** SM, **b** LM, and **c** loss factor on thermal treatment temperature for the S₂ and CML layers

heat treatment (Kim et al. 2014). The condensation reaction of lignin also leads to a decrease in its viscosity.

Comparing the data in Fig. 7 shows that the SM, LM, and loss factor of the S_2 layer are larger than those of the CML. The SM difference between the S_2 and CML layers results from the higher cellulose and smaller microfibril angle in the S_2 layer. In addition, the ordered arrangement of cellulose microfibrils in the S_2 layer means that the cell wall has stable structures with lower mobility of molecular chains. This leads to an obvious viscous response and dissipated energy of the S_2 layer in viscoelastic deformation. So the LM and loss factor of the S_2 layer are also greater than those of the CML.

Conclusion

The differences in viscoelastic properties between the cell wall S_2 and CML layers of thermally treated wood at 160–220 °C were evaluated by creep testing and dynamic modulus mapping of nanoindentation. The elastic parameters of cell walls, such as the reduced modulus K_1 of the Burger model and the storage modulus decrease and then increase as the treatment temperature increases, with minima occurring at 180 °C. The loss moduli and loss factors of the S_2 and CML layers decrease as the treatment temperature increases. The changes of viscoelastic properties with thermal treatment are related mainly to hemicellulose degradation, cross-linkage breakage, and cellulose microfibrils arrangement. In addition, creep compliance results indicate that the S_2 layer of the untreated and treated samples exhibited greater elasticity than the CML, although the rheological characteristics of the latter are more obvious. Finally, the loss modulus and loss factor of the S_2 layer were also both larger than those of the CML.

Supplementary Information The online version contains supplementary material available at <https://doi.org/10.1007/s00226-022-01409-7>.

Acknowledgements This work was financially supported by the Nature Science Foundation of China (No.32101458), the Guangxi Natural Science Foundation (Grant No. 2018GXNSFBA281108) and the Fundamental Research Funds for the Central Universities (D5000210672).

Author's contributions **DW**: Conceptualization, Methodology, Investigation, Formal analysis, Writing—original draft, Visualization. **EX**: Conceptualization, Methodology, Investigation, Formal analysis, Writing—original draft, Visualization. **DW** and **EX** contributed equally to this work and should be considered co-first authors. **LL**: Conceptualization, Writing—review and editing. **FF**: Conceptualization, Writing—review and editing.

Declarations

Conflict of interest The authors declare that they have no conflict of interest.

References

Åkerholm M, Salmén L (2003) The oriented structure of lignin and its viscoelastic properties studied by static and dynamic FT-IR spectroscopy. *Holzforschung* 57:459–465

- Barthelat F, Zhen Y, Buehler MJ (2016) Structure and mechanics of interfaces in biological materials. *Nat Rev Mater* 1:16007. <https://doi.org/10.1038/natrevmats.2016.7>
- Berglund J, Mikkelsen D, Flanagan BM, Dhital S, Vilaplana F (2020) Wood hemicelluloses exert distinct biomechanical contributions to cellulose fibrillar networks. *Nat Commun* 11:4692. <https://doi.org/10.1038/s41467-020-18390-z>
- Bekhta P, Niemz P (2003) Effect of high temperature on the change in color, dimensional stability and mechanical properties of spruce wood. *Holzforschung* 57:539–546. <https://doi.org/10.1515/HF.2003.080>
- Candelier K, Thevenon MF, Petrissans A, Dumarçay S, Gerardin P, Petrissans M (2016) Control of wood thermal treatment and its effects on decay resistance: a review. *Ann Forest Sci* 73:571–583. <https://doi.org/10.1007/s13595-016-0541-x>
- Chen S, Obataya E, Matsuo-Ueda M (2018) Shape fixation of compressed wood by steaming: a mechanism of shape fixation by rearrangement of crystalline cellulose. *Wood Sci Technol* 52:1229–1241. <https://doi.org/10.1007/s00226-018-1026-x>
- Ding T, Li GT (2011) Influence of steam pressure on physical and mechanical properties of heat-treated Mongolian pine lumber. *Eur J Wood Prod* 69:121–131. <https://doi.org/10.1007/s00107-009-0406-1>
- Esteves BM, Pereira HM (2009) Wood modification by heat treatment: a review. *BioResources* 4:370–404. <https://doi.org/10.1515/HF.2009.036>
- Esteves B, Graga J, Pereira H (2008) Extractive composition and summative chemical analysis of thermally treated eucalypt wood. *Holzforschung* 62:344–351
- Gong M, Lamason C, Li L (2010) Interactive effect of surface densification and post-heat-treatment on aspen wood. *J Mater Process Tech* 210:293–296. <https://doi.org/10.1016/j.jmatprotec.2009.09.013>
- Guo J, Song K, Salmén L, Yin Y (2015) Changes of wood cell walls in response to hygro-mechanical steam treatment. *Carbohydr Polym* 115:207–214. <https://doi.org/10.1016/j.carbpol.2014.08.040>
- Hill CAS (2006) Thermal modification of wood. In: Hill CAS (ed) *Wood modification: chemical, thermal and other processes*. John Wiley & Sons, pp 99–126
- Hori R, Wada M (2005) The thermal expansion of wood cellulose crystals. *Cellulose* 12:479–484. <https://doi.org/10.1007/s10570-005-5967-5>
- Kim J-Y, Hwang H, Oh S, Kim Y-S, Kim U-J, Choi JW (2014) Investigation of structural modification and thermal characteristics of lignin after heat treatment. *Int J Biol Macromol* 66:57–65. <https://doi.org/10.1016/j.ijbiomac.2014.02.013>
- Gril J, Hunt D, Thibaut B (2004) Using wood creep data to discuss the contribution of cell-wall reinforcing material. *C R Biol* 327:881–888. <https://doi.org/10.1016/j.crvi.2004.08.002>
- Kačková D, Kačík F, Čabalová I, Đurković J (2013) Effects of thermal treatment on chemical, mechanical and colour traits in Norway spruce wood. *Bioresource Technol* 144:669–674. <https://doi.org/10.1016/j.biortech.2013.06.110>
- Jin K, Qin Z, Buehler MJ (2015) Molecular deformation mechanisms of the woodcell wall material. *J Mech Behav Biomed* 42:198–206. <https://doi.org/10.1016/j.jmbbm.2014.11.010>
- Kubojima Y, Shida S, Okano T (1998) Mechanical and chromatic properties of high-temperature-dried sugi wood. *Wood Ind* 53:115–119
- Laine K, Segerholm K, Wälinder M, Rautkari L, Hughes M (2016) Wood densification and thermal modification: hardness, set-recovery and micromorphology. *Wood Sci Technol* 50:883–894. <https://doi.org/10.1007/s00226-016-0835-z>
- Li Y, Huang C, Li W, Wang S, Wang X (2017) The effects of thermal treatment on the nanomechanical behaviour of bamboo (*Phyllostachys pubescens* Mazel ex H. de Lahaie) cell walls observed by nanoindentation, XRD, and wet chemistry. *Holzforschung* 71:129–135. <https://doi.org/10.1515/hf-2016-0124>
- Mastouri A, Efhamisisi D, Shirmohammadli Y, Oladi R (2021) Physicochemical properties of thermally treated poplar wood in silicone and rapeseed oils: A comparative study. *J Build Eng* 43:102511. <https://doi.org/10.1016/j.jobe.2021.102511>
- Meng Y, Xia Y, Young TM, Cai Z, Wang S (2015) Viscoelasticity of wood cell walls with different moisture content as measured by nanoindentation. *RSC Adv* 5:47538–47547. <https://doi.org/10.1039/C5RA05822H>
- Nguila Inari G, Mounquengui S, Dumarçay S, Pétrissans M, Gerardin P (2007) Evidence of char formation during wood heat treatment by mild pyrolysis. *Polym Degrad Stabil* 92:997–1002. <https://doi.org/10.1016/j.polymdegradstab.2007.03.003>
- Qin L, Lin L, Fu F, Fan M (2018) Micromechanical properties of wood cell wall and interface compound middle lamella using quasi-static nanoindentation and dynamic modulus mapping. *J Mater Sci* 53:549–558. <https://doi.org/10.1007/s10853-017-1185-4>

- Rautkari L, Honkanen J, Hill CAS, Ridley-Ellis D, Hughes M (2014) Mechanical and physical properties of thermally modified Scots pine wood in high pressure reactor under saturated steam at 120, 150 and 180 °C. *Eur J Wood Prod* 72:33–41. <https://doi.org/10.1007/s00107-013-0749-5>
- Shen DK, Gu S, Bridgwater AV (2010) The thermal performance of the polysaccharides extracted from hardwood: Cellulose and hemicellulose. *Carbohydr Polym* 82:39–45. <https://doi.org/10.1016/j.carbpol.2010.04.018>
- Stanzl-Tschegg S, Beikircher W, Loidl D (2009) Comparison of mechanical properties of thermally modified wood at growth ring and cell wall level by means of instrumented indentation tests. *Holzforschung* 63:443–448. <https://doi.org/10.1515/HF.2009.085>
- Tjeerdsmas BF, Militz H (2005) Chemical changes in hydrothermal treated wood: FTIR analysis of combined hydrothermal and dry heat-treated wood. *Holz Roh- Werkst* 63:102–111. <https://doi.org/10.1007/s00107-004-0532-8>
- Tümen I, Aydemir D, Gündüz G, Üner B, Cetin H (2010) Changes in the chemical structure of thermally treated wood. *Bioresources* 5: 1936–1944. Doi: <https://doi.org/10.15376/biores.5.3.1936-1944>
- Tuong VM, Li J (2010) Effect of heat treatment on the change in color and dimensional stability of acacia hybrid wood. *BioResources* 5:1257–1267. <https://doi.org/10.1007/s00226-009-0268-z>
- Wang D, Lin L, Fu F (2019) The difference of creep compliance for wood cell wall CML and secondary S2 layer by nanoindentation. *Mech Time-Depend Mat* 2019:1–12. <https://doi.org/10.1007/s11043-019-09436-x>
- Wang D, Fu F, Lin L (2022) Molecular-level characterization of changes in the mechanical properties of wood in response to thermal treatment. *Cellulose*. <https://doi.org/10.1007/s10570-022-04471-3>
- Wang X, Deng Y, Wang S, Min C, Meng Y, Pham T, Ying Y (2014) Evaluation of the effects of compression combined with heat treatment by nanoindentation (NI) of poplar cell walls. *Holzforschung* 68:167–173. <https://doi.org/10.1515/hf-2013-0084>
- Wang X, Chen X, Xie X, Yan W, Wang S (2018) Effects of thermal modification on the physical, chemical and micromechanical properties of masson pine wood (*Pinus massoniana* lamb.). *Holzforschung* 72:1–8. <https://doi.org/10.1515/hf-2017-0205>
- Windeisen E, Bächle H, Zimmer B, Wegener G (2009) Relations between chemical changes and mechanical properties of thermally treated wood 10th EWLP, Stockholm, Sweden, August 25–28, 2008. *Holz-forschung* 63:773–778. <https://doi.org/10.1515/HF.2009.084>
- Wu Y, Zhang H, Zhang Y, Wang S, Wang X, Xu D, Liu X (2019) Effects of thermal treatment on the mechanical properties of Larch (*Larix gmelinii*) and Red Oak (*Quercus rubra*) wood cell walls via nanoindentation. *BioResources* 14:8048–8057
- Xiang E, Huang R, Yang S (2021) Change in micromechanical behavior of surface densified wood cell walls in response to superheated steam treatment. *Forests* 12:693. <https://doi.org/10.3390/f12060693>
- Xing D, Li J, Wang XZ, Wang SQ (2016) In situ measurement of heat-treated wood cell wall at elevated temperature by nanoindentation. *Ind Crop Prod* 87:142–149. <https://doi.org/10.1016/j.indcrop.2016.04.017>
- Xing D, Li J, Wang S (2020) Comparison of the chemical and micromechanical properties of Larix spp. after eco-friendly heat treatments measured by in situ nanoindentation. *Sci Rep-UK* 10: 4358. Doi: <https://doi.org/10.1038/s41598-020-61314-6>
- Xing D, Wang X, Wang S (2021) Temperature-dependent creep behavior and quasi-static mechanical properties of heat-treated wood. *Forests* 12:968. <https://doi.org/10.3390/f12080968>
- Yildiz S, Gezer ED, Yildiz UC (2006) Mechanical and chemical behavior of spruce wood modified by heat. *Bldg Environ* 41:1762–1766. <https://doi.org/10.1016/j.buildenv.2005.07.017>
- Yin YF, Berglund L, Salmén L (2011) Effect of steam treatment on the properties of wood cell walls. *Bio-macromol* 12:194–202. <https://doi.org/10.1021/bm101144m>
- Yin JP, Yuan TQ, Yun L, Song KL, Li HY, Zhao GJ, Yin YF (2017) Effect of compression combined with steam treatment on the porosity, chemical composition and cellulose crystalline structure of wood cell walls. *Carbohydr Polym* 155:163–172

Publisher's Note Springer Nature remains neutral with regard to jurisdictional claims in published maps and institutional affiliations.

Springer Nature or its licensor holds exclusive rights to this article under a publishing agreement with the author(s) or other rightsholder(s); author self-archiving of the accepted manuscript version of this article is solely governed by the terms of such publishing agreement and applicable law.